communications biology

A Nature Portfolio journal

Article

https://doi.org/10.1038/s42003-025-08139-z

Krüppel like factor 7 regulates mitochondrial dynamics balance in myocardial infarction

Cao Wang[1,5], Fuxing Zhu[1,5], Lan Zhou[2], Situo Zhang[1], Ruiqi Wang[1], Hui Tian[1], Bosong Zhang[1], Jiahui Wu[1], Xiang Xu[1], Ruixian Jiang[1], Xiaolu Hou[3], Jian Liu[4,6] & Weiming Tian[1,6]

Targeting the balance of mitochondrial fission and fusion can effectively alleviate the cardiac energy supply efficiency, to restore cardiac systolic dysfunction and reduce mortality. We previously found that *Klf7* is closely related to cardiac energy metabolism. Here we generated cardiomyocyte-specific *Klf7* knockout and overexpression mice that underwent myocardial infarction (MI) surgery. *Klf7* expression increased in the ischemic myocardium of mice, and cardiomyocyte-specific knockout *Klf7* significantly lowered the mortality of MI-inflicted mice and improved ATP insufficiency in MI. Subsequently, *Klf7* overexpression aggravated adverse cardiac remodeling and mitochondrial fission and fusion imbalance after MI. Our results also demonstrated that *Klf7* inhibited mitochondrial fusion and promoted mitochondrial fission by targeting prohibitin 2 (*Phb2*) and mitofusin 2 (*Mfn2*). Our study revealed a crucial role in upholding the overall balance of mitochondrial fission and fusion during MI. Furthermore, our findings indicated that the *Klf7*/*Mfn2*/*Phb2* axis holds promise as a potential target for therapeutic interventions of MI.

Myocardial infarction (MI) and the frequently subsequent heart failure (HF) are among the main causes of death worldwide, accounting for 23.6 million deaths annually[1]. Consequently, new strategies are required to protect the heart against myocardial infarct size, retain cardiac function, and improve patient outcome. Mitochondrial fission and fusion play crucial roles as arbiters of cardiac energy requirements, and an imbalance in mitochondrial fission and fusion contributes to the formation of fragmented mitochondria that fail to produce enough ATP for the heart under ischemic injury and HF, and impairs myocardial contraction and relaxation[2–4]. A previous study confirmed that mitochondrial fission and fusion balance are disrupted in HF patients and rodent model[5–7]. Overall, mitochondrial fission and fusion are profoundly altered after MI, with significant activation of the former and pathological disruption of the latter[8]. In addition, the process of differentiation from cardiac stem cells to adult cardiomyocytes requires changes in mitochondrial function and fission/fusion to accommodate the increased metabolic demands of differentiated beating cardiomyocyte[9], and the presence of mitochondrial fission or fusion is required in the development of the heart[10,11]. Therefore, the balance between mitochondrial fission and fusion is regarded as a major contributor to both physiological and pathological cardiac processes.

The dynamic processes of mitochondrial fission and fusion, which dictate the mitochondrial shape and influence ATP production, are tightly regulated. The mitochondrial network contains multiple proteins that promote mitochondrial fission, such as mitochondrial fission factor (MFF), mitochondrial fission 1 protein (FIS1), and dynamin-related protein 1 (DRP1), and fusion proteins such as mitofusin 1 (MFN1), mitofusin 2 (MFN2), and optic atrophy protein 1 (OPA1)[12]. As the main effector of mitochondrial fission, DRP1 has been the most studied in ischemic cardiomyopathy, and many authors have reported excessive activation of DRP1 and consequent mitochondrial fragmentation[7,13,14]. Our knowledge of the mechanisms regulating mitochondrial fission, primarily via DRP1, or regulating fusion, primarily via MFN1/MFN2, and the mechanisms regulating the mitochondrial dynamics balance remain poorly understood. Based on several evidence showing that genetic or pharmacological modulation of mitochondrial dynamics can confer resistance to ischemic burden, limit the area of myocardial infarction (MI), and delay the progression of cardiac adverse remodeling[15–18], improves left ventricular function[19], and reduces mortality upon MI[20]. However, therapeutic approaches for MI or HF using inhibitors of mitochondrial fission/fusion remain controversial and challenging[8]. The current potential for using mitochondrial fission and

[1]School of Life Science and Technology, Harbin Institute of Technology, Harbin, 150080, China. [2]The Second Affiliated Hospital of Heilongjiang University of Chinese Medicine, 150001, ChinaHarbin. [3]Department of Cardiology, The Fourth Affiliated Hospital of Harbin Medical University, Harbin, 150081, China. [4]School of Instrumentation Science and Engineering, Harbin Institute of Technology, Harbin, 150080, China. [5]These authors contributed equally: Cao Wang, Fuxing Zhu. [6]These authors Jointly supervised this work: Jian Liu, Weiming Tian. e-mail: tianweiming@hit.edu.cn

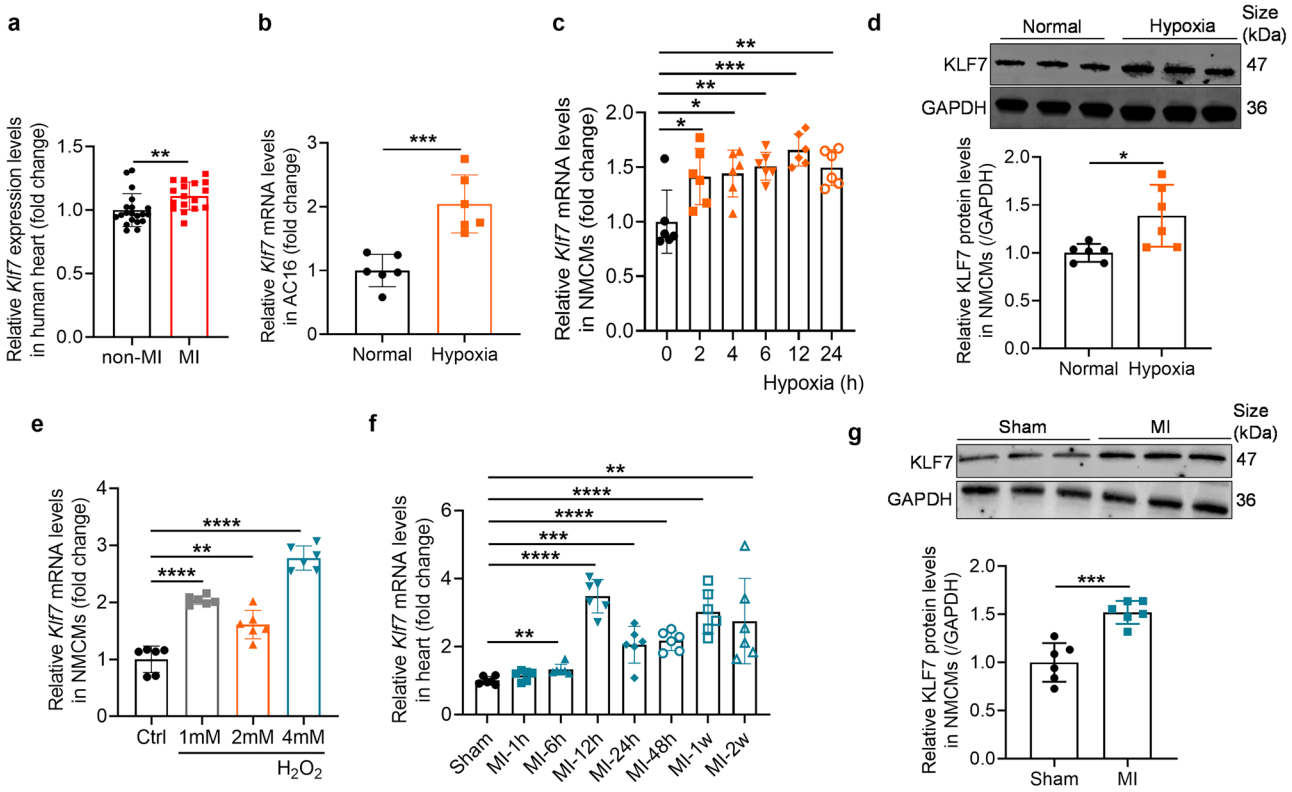

Fig. 1 | Upregulation of KLF7 expression in hypoxic cardiomyocytes and ischemic heart. a The expression of *Klf7* in aortic wall tissue of patients with ischemic cardiomyopathy was higher than controls ($n = 17$). **b** Increase in *Klf7* expression in AC16 cells after hypoxia treatment for 12 h ($n = 6$). **c** mRNA expression levels of *Klf7* in NMCMs cultured under hypoxic condition for the indicated time points ($n = 6$). **d** Increase in KLF7 protein levels in NMCMs after hypoxia treatment for 12 h ($n = 6$). **e** mRNA expression levels of *Klf7* in NMCMs treated with H_2O_2 for 24 h ($n = 6$). **f** *Klf7* mRNA expression levels in the heart of mice at the indicated time points post-MI ($n = 6$). **g** Elevation of cardiac KLF7 protein levels in the border zone of mice 2d after MI. ($n = 6$). In all panels, data are depicted as the mean ± SEM. $^{*}P < 0.05$, $^{**}P < 0.01$, $^{***}P < 0.001$, $^{****}P < 0.0001$, statistical significance was determined using unpaired, two-sided t-test.

fusion as a therapeutic strategy is limited to acute treatment, such as modulating mitochondrial dynamics on a chronic basis. It is uncertain whether inhibiting mitochondrial fission or activating mitochondrial fusion is harmful in the long term[21–23]. The balance between mitochondrial fission and fusion seems to be more important than merely inhibiting fission or activating fusion for the sake of mitochondrial health[22]. Above all, there is an urgent need to better understand the underlying mechanisms during MI, and HF regulation of mitochondrial fission and fusion balance will provide critical insights into therapeutic targeting of these processes.

In our study, the transcriptional factor *Klf7* was previously reported to be involved in the energy supply of cardiac glycolysis and fatty acid oxidation metabolism[24], thereby indicating that *Klf7* may be involved in the regulation of mitochondrial fission and fusion imbalance induced by MI. Herein, we report that mice with cardiomyocyte-specific *Klf7* deletion can alleviate ischemic HF, whereas overexpression of *Klf7* in adults can aggravate the pathological process of ischemic HF. In addition, our results demonstrate that *Klf7* negatively regulates *Mfn2* and *Phb2*, which aggravate the mitochondrial fission and fusion imbalance in vivo and in vitro under hypoxic condition, resulting in cardiomyocyte ATP deficiency and cardiac contractile dysfunction in mice. Our results point to a central role in maintaining the overall balance of mitochondrial fission and fusion in MI, and, more importantly, suggest that the *Klf7*/*Mfn2*/*Phb2* axis can be used as a potential therapeutic intervention target for MI.

Results

Cardiac *Klf7* expression is increased in the ischemic or hypoxic models both in vivo and in vitro

To investigate the role of *Klf7* in MI, we analyzed the myocardial tissue microarray sequencing database (GSE83500)[25] in patients with ischemic cardiomyopathy, and it revealed that *Klf7* expression was significantly upregulated in the hearts of patients with MI (Fig. 1a). We then measured *Klf7* expression under pathological hypoxic conditions. We cultured adult human ventricular cardiomyocyte AC16 cells under hypoxic conditions and performed cardiac mRNA analysis, which showed that *Klf7* was upregulated 2-fold after exposure to hypoxic conditions (Fig. 1b). The regulation of *Klf7* in cultured mouse cardiomyocytes injured by hypoxia or H_2O_2 was then investigated. Consistently, *Klf7* mRNA and KLF7 protein levels were significantly increased in cardiomyocytes exposed to hypoxia for 12 h (Fig. 1c, d) and to H_2O_2 (Fig. 1e). We then prepared C57BL/6 mice at the age of 8 weeks with MI by permanently ligating the left coronary artery and found that *Klf7* mRNA expression levels were upregulated for 6 h and sustained to 2 weeks post-MI (Fig. 1f). KLF7 protein and transcript levels were increased in the hearts of mice 2d post-MI (Fig. 1g). These data indicate that *Klf7* is involved in the pathogenesis of ischemic and hypoxic models both in vivo and in vitro.

Cardiomyocyte-specific *Klf7* deletion improves the imbalance of mitochondrial fission and fusion and ATP production induced by myocardial infarction

Our previous study found that *Klf7* plays an important role in regulating energy metabolism in the heart[24], given the crucial role that mitochondria play in generating ATP to maintain normal heart contractile function. We further explored whether *Klf7* affects the respiratory capacity and mitochondrial dynamics induced by MI. We generated cardiomyocyte-specific *Klf7* KO mice ($Klf7^{flox/flox}$/Myh6 Cre) as described previously[24] and randomized them to undergo MI or sham surgery. Based on the results of the Seahorse XFe24 experiments, KO mice exhibited improved ATP production, maximal respiratory levels, and

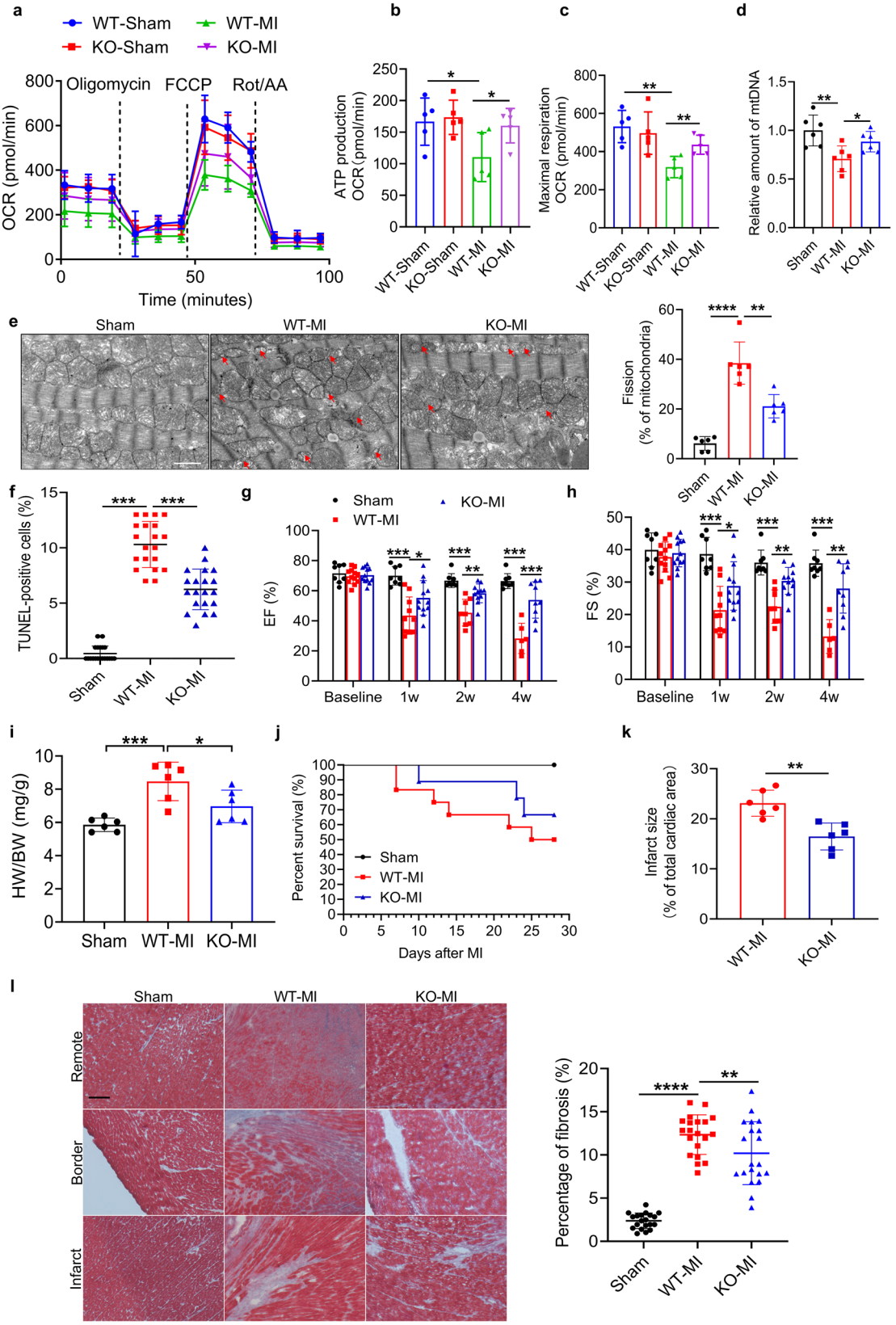

relative amount of mitochondrial DNA following MI (Fig. 2a–d), thereby suggesting that the deletion of *Klf7* may alleviate mitochondrial insufficiency induced by MI. Next, we examined the mitochondrial network in vivo upon MI, and the results are shown in Fig. 2e. Electron microscopy revealed that mitochondria in the hearts of sham-operated mice were of similar size, whereas MI resulted in smaller mitochondria and an increased percentage of fission in WT mice, but this effect was attenuated in KO mice. Moreover, *Klf7* deletion decreased the percentage of cardiomyocyte apoptosis induced by MI (Fig. 2f and Supplementary Fig. 1a, b).

Fig. 2 | Cardiomyocyte-specific *Klf7* deletion alleviates cardiac and mitochondrial dysfunction after myocardial infarction. a OCR of isolated cardiac mitochondria at 1-week post MI surgery ($n = 5$). **b**, **c** Quantification of ATP production and maximal respiration rate ($n = 5$). **d** Relative amount of mitochondrial DNA in mouse heart ($n = 6$). **e** Representative TEM images of heart tissue and counting of fragmented mitochondria showed that *Klf7* deletion attenuates mitochondrial fission upon MI. Red arrows indicate fragmented mitochondria. Scale bar, 1 μm ($n = 6$). **f** *Klf7* deletion attenuates apoptosis of cardiomyocytes in the border zone ($n = 4$ mice/group, 5 sections/mouse). Representative parasternal long-axis measurements of ejection fraction (**g**) and fractional shortening (**h**) in WT and KO mice under MI surgery ($n = 6$–12). **i** HW/BW in KO mice subjected to MI surgery ($n = 6$). **j** Kaplan–Meier survival curve for mice subjected to MI or sham surgery with cardiomyocyte-specific deletion of *Klf7* ($n = 12$). **k** Quantification of infarct size as percentage of total cardiac area in WT and KO mice after sham or MI surgery ($n = 6$). **l** Quantitative evaluation of interstitial fibrosis in WT and KO mice challenged with MI. Scale bar, 100 μm ($n = 4$ mice/group, 5 sections/mouse). In all panels, data are presented as mean ± SEM. $^{*}P < 0.05$, $^{**}P < 0.01$, $^{***}P < 0.001$, $^{****}P < 0.0001$, statistical significance was determined using unpaired, two-sided t-test. HW/BW, heart weight normalized to body weight.

Cardiac 2D echocardiography analysis at baseline and 1, 2, and 4 weeks post MI (Supplementary Fig. 2a) showed no differences at baseline, but higher ejection fraction (EF) and fraction shortening (FS) in KO mice with MI beginning 1 week after MI, compared to WT mice post-MI (Fig. 2g, h). WT-MI mice showed a significant decrease in left ventricular posterior wall thickness (LVPW), interventricular septum thickness (IVS), systolic left ventricular volume (LVvols), and systolic left ventricular internal diameter (LVIDs) at diastole and systole, which was improved in KO mice with MI (Supplementary Fig. 2b–i). There was no significant difference in the diastolic left ventricular volume (LVvold) and diastolic left ventricular internal diameter (LVIDd) at diastole and systole between KO and WT mice post-MI (Supplementary Fig. 2b–i). Furthermore, the increase in heart weight normalized to body weight (HW/BW) was suppressed in KO mice with MI (Fig. 2i). Consistently, cardiomyocyte-specific knockout of *Klf7* resulted in significantly-reduced mortality (Fig. 2j). The hearts of cardiomyocyte-specific *Klf7* KO mice had a smaller infarct size (Fig. 2k), lesser left ventricular fibrosis, and better cardiomyocyte arrangement than WT mice post-MI (Fig. 2l, Supplementary Fig. 2j). Based on the previous observation that *Klf7* stimulation coincides with *Klf5* upregulation and *Klf15* downregulation, these changes have been associated with HF and metabolic comorbidities[26,27]. Accordingly, we examined the effect of *Klf7* KO mice on the expression of *Klf5* and *Klf15* in the heart of mice with MI. The results showed that compared with WT-MI mice, *Klf7* knockout had no significant effect on the expression of *Klf5* and *Klf15* in the infarct border zone (Supplementary Fig. 2k, l). Hence, the effect of *Klf7* on MI may be independent of *Klf5* and *Klf15*. In conclusion, cardiomyocyte-specific deletion of *Klf7* can substantially improve MI-induced deterioration of mitochondrial and cardiac functions.

Knockdown of *Klf7* in cardiomyocytes improves the imbalance of mitochondrial fission and fusion and ATP production under hypoxic condition

To further describe the effect of *Klf7* on the metabolic potential of hypoxic cardiomyocytes, we recorded ATP production and maximal respiration in cardiomyocytes after 1 mM of H_2O_2 treatment. Compared to the H_2O_2-treated group, ATP levels and maximal respiration in the *Klf7* knockdown group showed a trend of improvement, but there was no significant difference (Fig. 3a–c, Supplementary Fig. 3). Our results also showed that *Klf7* knockdown could reduce mitochondrial fragmentation and thus promote mitochondrial fusion upon hypoxia in the cellular model (Fig. 3d–f). Hypoxia induced cardiomyocyte apoptosis, which, however, was alleviated by *Klf7* knockdown (Fig. 3g–i). In hypoxic conditions, knockdown of *Klf7* in cardiomyocytes decreased the expression of apoptosis genes compared with the controls (Supplementary Fig. 1c, d). These results confirm that Klf7 deletion alleviates cardiac injury and indicate that this is associated with decreased mitochondrial fission both in vivo and in vitro.

Cardiomyocyte-specific *Klf7* overexpression aggravates systolic dysfunction and mitochondrial dynamics imbalance induced by myocardial infarction or hypoxia

To further verify the effect of cardiac *Klf7* on mitochondrial dynamic balance, we overexpressed *Klf7* in mice with adeno-associated virus serotype 9 (AAV9) to assess the effect of cardiac *Klf7*. Western blotting revealed that cardiomyocyte-specific constitutive KLF7 expression was apparent after 3 weeks of AAV9-*Klf7* treatment (Fig. 4a). 2D echocardiography analysis with whole ventricle tracing (Supplementary Fig. 4a) showed that *Klf7* overexpression significantly decreased EF and FS at 4 weeks after MI surgery, and aggravated cardiac dysfunction induced by MI compared with the controls (Fig. 4b, c and Supplementary Fig. 4b–i). Compared with the AAV-negative control-MI (AAV-NC-MI) mice, the HW/BW ratio was evaluated 4 weeks post-MI in AAV-*Klf7* mice (Fig. 4d). *Klf7* overexpression aggravated the disordered myocardial tissue arrangement, increased myofilament gaps, and fibrosis in the left ventricle border and infarct tissue caused by MI, as revealed by histological examination (Fig. 4e, Supplementary Fig. 4j). Overexpression of *Klf7* also increased MI-induced infarct size (Supplementary Fig. 4k). Mitochondria in the hearts of MI-operated AAV-NC mice decreased in size related to the sham mice, but this effect was aggravated in AAV-*Klf7* mice, indicating increased mitochondrial fission or decreased mitochondrial fusion balance upon *Klf7* overexpression (Fig. 4f). Strikingly, AAV-*Klf7* mice exhibited decreased relative amount of mitochondrial DNA following MI (Fig. 4g). Furthermore, MI mice displayed increased levels of $TUNEL^{+}$ cardiomyocytes, which were greater in AAV-*Klf7* mice than in AAV-NC mice (Fig. 4h). Similar to the AAV-NC mice with MI, cardiomyocyte *Klf7* overexpression increased Bax mRNA expression and decreased Bcl-2 mRNA expression levels (Supplementary Fig. 4l). More importantly, overexpression of *Klf7* in cardiomyocytes resulted in impaired ATP production and maximal respiratory capacity in mitochondria isolated from mouse hearts after MI (Fig. 4i, j).

We also tested the effects of overexpression of *Klf7* on mitochondrial dynamics and ATP levels in HL-1 cells. For this, we subjected cardiomyocytes using the *Klf7* lentivirus to hypoxia in combination with H_2O_2 treatment. Indeed, ATP production was lower following the overexpression of *Klf7* in HL-1 cells compared to the control group after H_2O_2 treatment (Fig. 5a, b, Supplementary Fig. 5a). However, maximal respiration showed a trend of decrease, but there was no significant difference (Fig. 5a, c, Supplementary Fig. 5a). As shown in Fig. 5d–f, mitochondrial fragmentation occurred in response to hypoxia and *Klf7* overexpression promoted this fragmentation further. Furthermore, our results showed that hypoxia-induced cardiomyocyte apoptosis was augmented by *Klf7* overexpression (Fig. 5g, h, Supplementary Fig. 5b). Altogether, these findings suggest that *Klf7*-enhanced cardiac injury is associated with increased mitochondrial fission.

Klf7 regulates mitochondrial dynamics balance by targeting both *Mfn2* and *Phb2*

To discover the mechanism by which *Klf7* regulates the balance of mitochondrial dynamics during the pathological process of MI, we examined the expression of genes involved in mitochondrial fusion and fission in response to *Klf7* depletion using qRT-PCR. As shown in Fig. 6a, *Mfn2*, *Phb2*, and *Fis1* were significantly upregulated in the hearts of *Klf7* KO mice compared to WT mice, while there was no significant difference among other genes. We also searched the target genes involved in mitochondrial dynamics in the ChIP-seq database[28] (https://doi.org/10.5281/zenodo.5243430), which showed that *Mfn1*, *Mfn2*, and *Phb2* are the target genes of *Klf7*. Among these genes, we rigorously selected *Mfn2* and *Phb2* as preliminary targets, by which *Klf7* may transcriptionally regulate mitochondrial homeostasis. Notably, *Phb2* has been reported to regulate diverse facets of mitochondrial

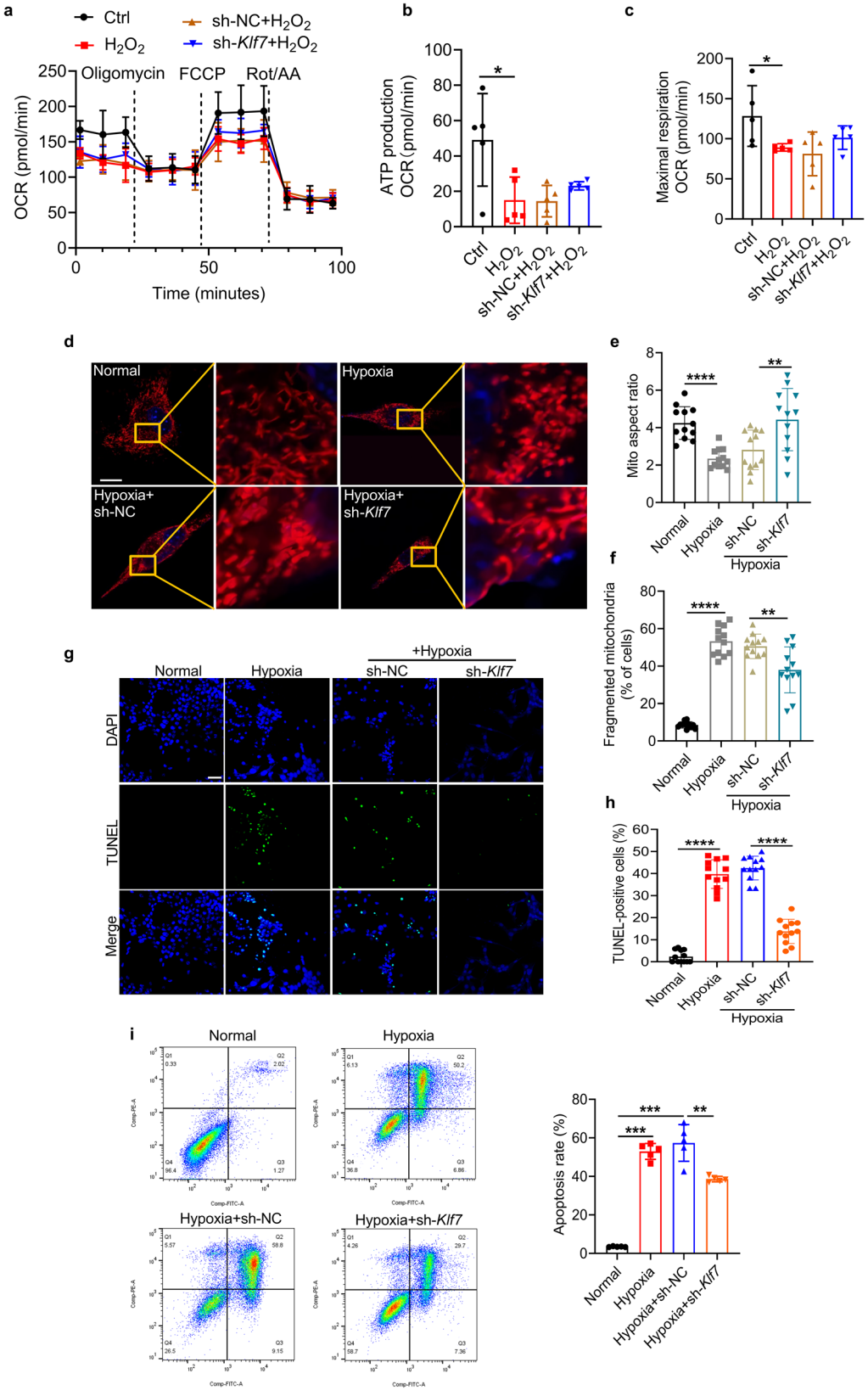

function, including mitochondrial respiration chain activity[29], promoting cristae morphogenesis[30] and mitochondrial mitophagy[31], and restricting mitochondrial fission[32,33]. Similarly, mouse *Mfn2*$^{-/-}$ hearts spontaneously develop dilated cardiomyopathy accompanied by impaired contractile function[26,34]. In this study, we used luciferase assays to examine the roles of *Mfn2* and *Phb2* as *Klf7* targets. Transfection of a plasmid containing the luciferase sequence followed by the *Mfn2* and *Phb2* promoter regions, together with a *Klf7* mimic, led to decreased normalized luciferase activity (Fig. 6b–g). Then, we performed chromatin immunoprecipitation-polymerase chain reaction (ChIP-PCR) analysis to compare the level of

Fig. 3 | Knockdown of *Klf7* alleviates cardiomyocyte mitochondrial dynamics imbalance and insufficient ATP supply under hypoxic condition. a–c OCR, ATP production, and maximal respiration rate of HL-1 cells treated with 1 mM H_2O_2 ($n = 5$). **d** NMCMs were stained with MitoTracker Red (red)/DAPI (blue). Representative images show the mitochondrial fission/fusion dynamics. Scale bar, 10 μm. **e**, **f** Quantitative analysis of the percentage of cells with mitochondria aspect ratio and fragmented mitochondria ($n = 12$). **g**, **h** HL-1 cells were transfected with lentiviral vectors for *Klf7* knockdown or its negative control for 48 h, followed by exposure to hypoxic conditions for an additional 12 h. Apoptosis was determined by the TUNEL assay. DAPI indicates the nucleus. Scale bar, 50 μm. Quantitative analysis of the percentage of apoptotic cells (12 randomly selected fields from 4 independent experiments). **i** Cell apoptosis and the average apoptotic rate of cardiomyocytes treated with lentiviral vectors for *Klf7* knockdown were assessed after exposure to hypoxic conditions for 12 h ($n = 5$). The x-axis labeled Comp-FITC-A indicates Annexin V, while the y-axis labeled Comp-PE-A indicates PI. In all panels, data are presented as mean ± SEM. $^{*}P < 0.05$, $^{**}P < 0.01$, $^{****}P < 0.0001$, statistical significance was determined using unpaired, two-sided t-test.

Mfn2 and *Phb2* enrichment in the complex pulled down with HA-tag antibody to that of anti-IgG control (Fig. 6h–j). Importantly, our data suggested that *Klf7* can simultaneously and negatively regulate *Mfn2* and *Phb2*. Moreover, our results showed that myocardial-specific *Klf7* KO can significantly restore the decreased expression of *Mfn2* and *Phb2* in myocardial tissue of mice perturbed by MI (Fig. 7a, b). In addition, *Klf7* knockdown partially prevented *Mfn2* and *Phb2* downregulation induced by hypoxic conditions in vitro (Supplementary Fig. 5c, d). Our results also showed that *Klf7* overexpression aggravated and disturbed the balance of *Mfn2* and *Phb2* expression in vivo and in vitro (Fig. 7c, d, Supplementary Fig. 5e, f).

Overexpression of *Mfn2* or *Phb2* alleviates mitochondrial dynamics imbalance in hypoxic cardiomyocytes upon *Klf7* overexpression

To determine whether *Klf7* plays a role in MI- or hypoxia-induced mitochondrial fission and fusion processes, we conducted in vitro and in vivo studies that evaluated the effect of the *Klf7*/*Mfn2*/*Phb2* axis on mitochondria and cardiac function. The result showed that exogenous overexpression of *Klf7* in hypoxic cardiomyocytes overexpressing *Mfn2* or *Phb2* increased the number of TUNEL-positive cells (Fig. 7e). Notably, *Mfn2* or *Phb2* overexpression was sufficient to attenuate the insufficient ATP energy supply of H_2O_2-treated cardiomyocytes, but overexpression of *Klf7* partially reversed the improvement effect (Fig. 7f, g). In addition, overexpression of *Klf7* in hypoxic cardiomyocytes overexpressing *Mfn2* or *Phb2* caused more fragmented mitochondria (Fig. 7h–l). Taken together, our results suggest that *Mfn2* and *Phb2* can mediate, or partially mediate the effects of *Klf7* on mitochondrial fission and fusion balance.

Cardiac-specific knockdown of *Mfn2* or *Phb2* aggravates cardiac dysfunction and mitochondrial dynamics imbalance in adult KO mice

As demonstrated above, adult *Klf7* KO mice were protected against MI imbalance in mitochondrial dynamics. We injected the tail veins of postnatal 8 weeks old *Klf7* KO mice with lentivirus of knockdown NC and *Mfn2* or *Phb2* for a total of 4 weeks. Subsequently, the mice were subjected to echocardiography (Fig. 8a). The expression levels of cardiomyocyte Mfn2 and Phb2 were reduced to 50% and 40%, respectively, by the injection of 3E + 11 AAV9 virus particles compared to their expression in the control group (Fig. 8b). However, the expression levels of *Mfn2* and *Phb2* in endothelial cells did not show significant changes (Fig. 8b). In *Klf7* KO mice, knockdown of *Mfn2* or *Phb2* significantly aggravated cardiac function induced by MI, as shown by EF and FS (Fig. 8c–e). Similar results were observed in WT mice (Fig. 8c–e). Other echocardiographic parameters appeared to be affected. Compared with the KO-AAV-NC group, the LVvol and LVID in systole and diastole of *Klf7* KO mice with *Mfn2* knockdown were significantly increased, and the LVPW in systole was significantly decreased. *Klf7* KO mice with *Phb2* knockdown displayed decreased LVPW in systole and diastole, and significantly increased LVvol and LVID in systole (Supplementary Fig. 6a–g). In conclusion, knocking down *Mfn2* or *Phb2* reversed the improvement of cardiac function in mice with MI by knockout *Klf7*.

We sought to assess the post-MI mitochondrial network using electron microscopy. Our findings demonstrated a reduction in the quantity of fragmented mitochondria in the hearts of *Klf7* KO mice in contrast to the WT mice under MI (Fig. 8f, g). Notably, this effect was exacerbated in KO-AAV-*Mfn2*/*Phb2* mice, suggesting a heightened level of mitochondrial fission or a diminished occurrence of mitochondrial fusion in these mice (Fig. 8f, g). We also performed the TUNEL and flow cytometry analysis to assess whether the observed knockdown of *Mfn2* and *Phb2* aggravates the MI-induced cardiomyocyte apoptosis in *Klf7* KO mice (Fig. 8h–j). Our results showed that knockdown of *Phb2* or *Mfn2* significantly increased apoptosis in the *Klf7* KO mice under MI. Similarly, there was a significant increase in cardiomyocyte apoptosis in WT-AAV-*Mfn2*/*Phb2* mice compared to WT-AAV-NC mice under MI (Fig. 8h–j). In addition, these findings correlated well with the observed *Bax* and *Bcl-2* mRNA levels (Fig. 8k). In sum, the above results indicate that myocardial-specific *Klf7* knockout improves the balance between mitochondrial fission and fusion in the heart, and this improvement was significantly diminished by downregulating *Phb2* or *Mfn2*. Taken together, these findings suggest that *Klf7* can simultaneously modulate the expression of *Mfn2* and *Phb2* to regulate cardiac homeostasis of mitochondrial dynamics and cardiac function.

Discussion

Despite notable progress in comprehending the dynamics of mitochondrial fission and fusion implicated in the development of MI and HF, specific mechanistic intricacies still remain elusive. Clinical studies have shown a significant increase in the expression of DRP1 in the tissues of HF patients with reduced ejection fraction, without differences in the expression of OPA1 and MFN2[5]. Additionally, OPA1 protein expression was reduced in human failing heart samples from adults presenting with ischemic cardiomyopathy, expression levels of MFN1, MFN2, and DRP1 were increased, whereas FIS1 expression was unchanged[27]. However, in the HF rat model, the expression levels of OPA1 were significantly decreased, while that of MFN1/MFN2, DRP1, and FIS1 were unchanged[27]. In summary, variations in the activity of mitochondrial fission and fusion proteins are also different due to the causes and stages of HF. Our study demonstrated that *Mfn2* and *Phb2* expression decreased in heart tissue during the early stages of MI. Studies have shown that the interactions between mitochondrial fission and fusion are complex, and loss of either fission-related or fusion-related proteins has been demonstrated to be detrimental to the heart. The optimal therapeutic strategy for patients with HF is not just to inhibit mitochondrial fission or activate mitochondrial fusion but rather to maintain a balance between the two processes. Targeting only mitochondrial fission or fusion is not sufficient for improving mitochondrial health[35]. The present study demonstrated that *Klf7* could simultaneously target and regulate *Mfn2* and *Phb2* to affect the dynamic balance of mitochondrial fission and fusion in cardiomyocytes independent of *Drp1*, thereby affecting cardiomyocyte energy supply after MI. It is important to maintain the overall balance of mitochondrial fission and fusion. Similarly, a study revealed that an imbalance between mitochondrial fission and fusion (in either direction) is more deleterious than the simultaneous abrogation of both processes[22]. This idea is supported by our finding that cardiomyocyte-specific knockout of *Klf7* promotes mitochondrial fusion and simultaneously inhibits fission by targeting *Mfn2* and *Phb2*. The *Klf7*/*Mfn2*/*Phb2* axis may shed new light on the complex molecular mechanism of mitochondrial fission and fusion dynamics.

An imbalance in mitochondrial fusion and fission can affect mitochondrial respiratory function and susceptibility to cell death in HF[36,37], and the genetic or pharmacological modulation of mitochondrial dynamics

confers resistance to ischemic injury[17–22]. Direct and indirect inhibition of DRP1 mostly reduces MI size and reactive oxygen species (ROS) levels in mouse models subjected to coronary artery occlusion and reperfusion damage[7,38]. Metformin exerts cardioprotective effects by attenuating mitochondrial dysfunction and decreasing DRP1 expression and cardiac apoptosis after acute cardiac ischemia and reperfusion (I/R) injury in rats[39]. Unfortunately, the relevant clinical study was terminated prematurely[8]. Mdivi-1, a DRP1 inhibitor, significantly reduced myocardial infarct size in vivo in murine heart[7]. Chronic inhibition of DRP1 is not suitable for therapeutic purposes as it produces excess superoxide, impairs mitochondrial respiration, and inhibits autophagy, thus limiting its potential use as a therapy for MI[40]. Among the therapeutic potential of improving

Fig. 4 | Cardiomyocyte-specific overexpression of *Klf7* aggravates cardiac and mitochondrial dysfunction induced by myocardial infarction. a Infection efficiency of mouse tail-vein injection of AAV9 for *Klf7* expression in cardiomyocytes and endothelial cells ($n = 6$). **b**, **c** Left ventricular ejection fraction and fractional shortening were measured by echocardiography ($n = 7$–12). **d** Quantification of the HW/BW ratio in AAV-NC and AAV-*Klf7* mice after sham or MI surgery ($n = 6$). **e** Representative images of Masson's trichrome-stained hearts from mice in the four groups and quantitative analysis of the extent of fibrosis. The area stained blue represents fibrosis, the area boxed in black represents the typical area of fibrosis, Scale bar, 100 μm ($n = 4$ mice/group, 6 sections/mouse). **f** TEM was performed to detect the ultrastructure of cardiomyocytes in heart tissues from mice treated with AAV-*Klf7* or AAV-NC after MI surgery. Red arrows indicate fragmented mitochondria. Scale bar, 1 μm ($n = 6$). **g** Relative amount of mitochondrial DNA in mouse heart tissues from mice treated with AAV-*Klf7* or AAV-NC after 1 week after MI surgery ($n = 6$). **h** Cardiomyocyte apoptosis in heart tissues from AAV-NC and AAV-*Klf7* mice after sham or MI surgery ($n = 4$ mice/group, 5 sections/mouse). **i** Oxygen consumption rate of isolated mouse cardiac mitochondria at 1 week after MI surgery. **j** Quantification of ATP production and maximal respiration rate of isolated mouse cardiac mitochondria at 1 week after MI surgery ($n = 5$). In all panels, data are depicted as the mean ± SEM. $^{*}P < 0.05$, $^{**}P < 0.01$, $^{***}P < 0.001$, $^{****}P < 0.0001$, statistical significance was determined using unpaired, two-sided t-test.

mitochondrial fusion, the mitochondrial fusion promoter M1 has been used in rats subjected to I/R, resulting in a reduction in MI size and the associated mortality[41]. There is substantial experimental evidence supporting the use of targeting mitochondrial fission or fusion as a potential therapeutic strategy to reduce the severity of MI injury. However, clinical trials have proven to be both controversial and challenging[8], while innovative approaches and new therapeutic targets are required. The primary cause of the pathological phenotype are genes rather than coding proteins. Transcription factors play a key role in regulating gene activity and can specifically modulate diseases due to their fundamental role in binding to the regulatory regions of genes, both in terms of status and quantity[42]. As a result, transcription factors function as drug targets that not only target the root cause of the pathological problem (the gene itself) but also address the side effects caused by crosstalk within signaling pathways. Emerging evidence suggests that some inhibitors such as JQ1[43], DRB[44], and valproic acid[45] target the transcriptional machinery in models of cardiac hypertrophy and ischemic injury. In the above, it is suggested that targeting transcriptional regulation provides a new perspective for the treatment of HF. In our study, we revealed that cardiomyocyte-specific knockout of *Klf7* significantly reduces the mortality of mice with MI, improves ATP insufficiency in heart-induced MI, and reduces the percentage of MI area, suggesting that *Klf7* may be a potential therapeutic target for mitochondrial metabolism and mitochondrial dynamics imbalance induced by MI or HF.

During MI, intense inflammatory responses and oxidative stress cause myocardial cell damage and substantial changes in cellular signaling pathways, which critically regulate the pathological mechanisms of MI[46]. To identify key regulatory factors related to MI, we utilized an online database (http://bioinfo.life.hust.edu.cn/HumanTFDB/#!)[47] to predict potential transcription factors that regulate *Klf7* expression. Additionally, we examined transcription factor expression changes during MI progression using various models from the GEO database (https://www.ncbi.nlm.nih.gov/geo). The analyzed models included patient aortic wall samples (GSE83500[25]), mouse myocardial tissues (GSE243668[48,49], GSE255826[50]), and mouse cardiomyocytes (GSE255933[51]). Comparative analysis of these datasets identified the transcription termination factor 2 (TTF2) as a potential key transcription factor influencing *Klf7* expression, and we will conduct detailed verification in the subsequent study.

Our study was confined to male mice aged 8–12 weeks and did not explore potential sex- or age-related variations in *Klf7* expression and mitochondrial fission/fusion. Given our emphasis on young mice, the applicability of our findings to older patient populations with MI or HF should be approached with caution. Our previous study demonstrated that cardiomyocyte-specific *Klf7* knockout mice developed spontaneous cardiac hypertrophy after 6 months and subsequently developed pathological HF[29]. Among cardiomyocyte-specific *Klf7*-deficient mice, we observed no adverse effects likely due to the fact that our study focused on young mice (2 months of age) who had normal cardiac function at that time. Moreover, in our previous study, the pathological progress of cardiac hypertrophy induced by the cardiomyocyte-specific overexpression of *Klf7* in the embryonic myocardium was spontaneous. Overexpression of *Klf7* promoted fatty acid oxidation and inhibited glycolysis, resulting in HF in the embryonic mouse heart due to insufficient energy supply. In this study, overexpression of *Klf7* in adult mice and cardiomyocytes was performed under hypoxia stimulation, which aggravated the phenomenon of insufficient energy supply of cardiomyocytes. Similarly, cardiomyocyte KLF5 inhibition exerts protective effects in ischemic HF, while fibroblast KLF5 drives pressure-overload hypertrophy[52]. Our previous study combined with our present findings suggests that the expression of *Klf7* may be different in various developmental cycles of the heart, which leads to distinct effects. Future studies are needed to clarify the specific effects and mechanisms of *Klf7* on mitochondrial function and metabolism during cardiac development.

In conclusion, our study identified *Klf7* as a central transcriptional regulator of mitochondrial fission and fusion. We uncovered a new mechanism by which *Klf7* simultaneously regulates *Mfn2* and *Phb2* genes, thus affecting mitochondrial fission/fusion dynamics equilibrium and cardiomyocyte energy supply insufficiency under MI injury, suggesting the importance of maintaining the overall balance of mitochondrial fission and fusion. Moreover, modulating the expression of *Klf7* may represent a potential therapeutic target for interventional treatment of MI and HF. This may also provide a new clue for understanding the *Klf7-mediated* mitochondrial homeostasis.

Methods

Animals

Male C57BL/6J mice (20 ± 2 g) were purchased from Changsheng Animal Ltd (Jilin, China). Cardiomyocyte-specific *Klf7* knockout (Myh6^{Cre}×*Klf7*$^{flox/flox}$, *Klf7*^{CKO}) mice were generated by Shanghai Cyagen Co., Ltd. (Shanghai, China) using CRISPR/Cas9 system in the C57BL/6J mouse background previously described[24]. Myh6^{Cre} mice refer to mice expressing a Cre recombinase transgene controlled by the Myh6 promoter, which is specifically active in the cardiomyocytes of adult mice. Experiments were performed with male mice for up to 2 months after left anterior descending coronary artery ligation, and wild-type (WT) littermates and C57BL/6J mice were used as controls. Mice were kept in a pathogen-free environment with a controlled 12 h light-dark cycle in a specific barrier facility. We have complied with all relevant ethical regulations for animal use, and all animal procedures were conducted in accordance with the guidelines set forth by the Harbin Institute of Technology Committee on Animal Resources (IACUC-2022054).

Hypoxic treatment

Hypoxia was performed as described previously[29]. Briefly, cells were placed in a hypoxic chamber with a water-saturated atmosphere composed of 5% CO_2 and 95% N_2 under hypoxic conditions for 12 h. The H_2O_2-treated group was treated with 100 μL of 1, 2, or 4 mmol. L^{-1} H_2O_2 for 24 h while the control group was treated with 100 μL of Dulbecco's modified Eagle medium (DMEM) medium (Gibco, Waltham, MA, USA).

Mitochondrial morphology detection in the cells

Mitochondrial staining was carried as others described with neonatal mice cardiomyocytes (NMCMs)[14,29]. NMCMs were cultured on coverslips. The cells were then incubated with MitoTracker Red (M22425, Thermo Fisher Scientific, Waltham, MA, USA) at 37 °C for 30 min. The cells were washed with PBS and then were fixed with 4% formaldehyde (Sigma-Aldrich, Waltham, MA, USA) for 15 min. Nuclei were stained with 4',6-diamidino-2-phenylindole dihydrochloride (DAPI, Solarbio, Beijing, China). Images were acquired using a confocal laser scanning microscope (LSM710; Carl Zeiss

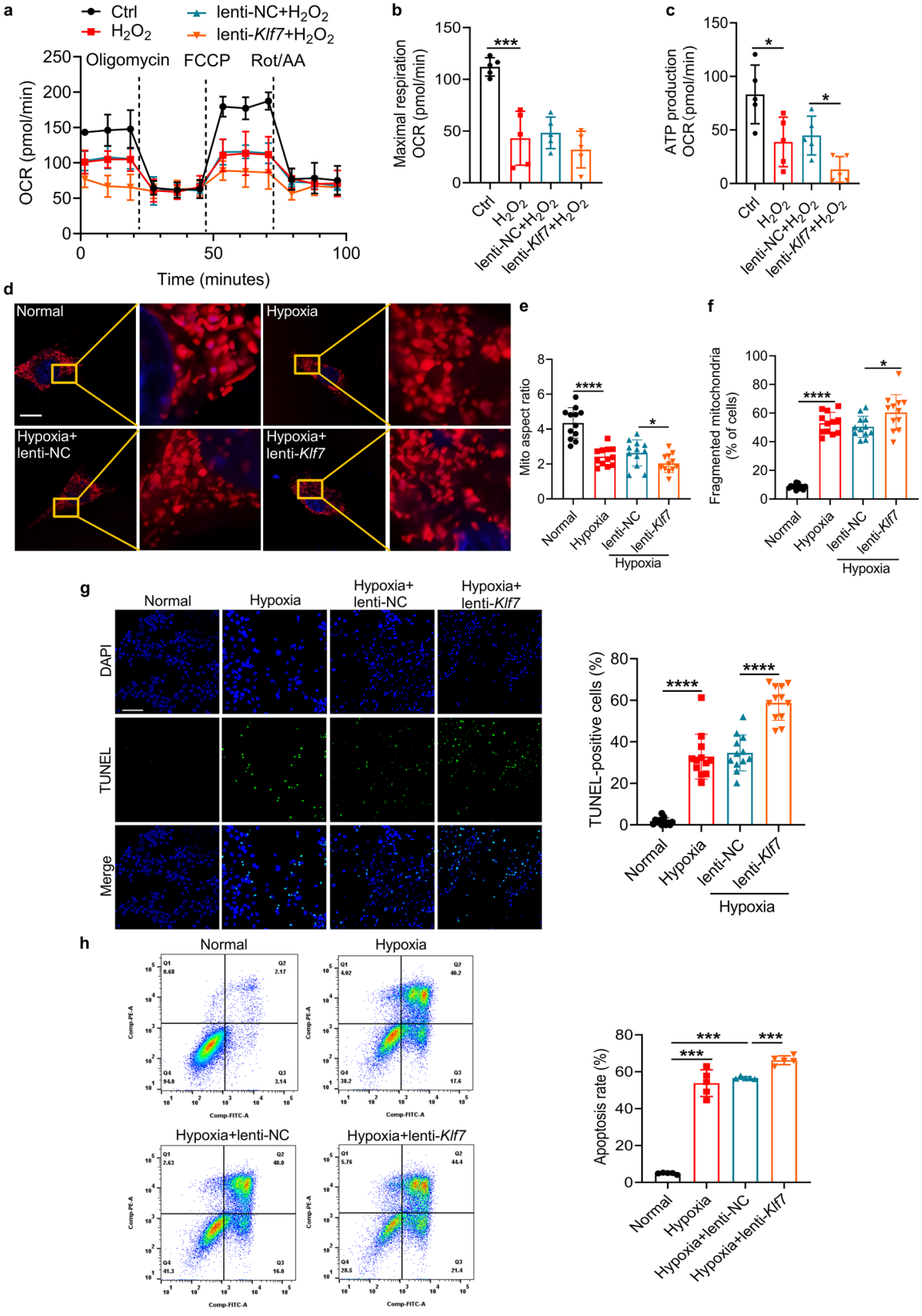

AG, Jena, Germany). Mitochondrial morphology was determined using ImageJ software (National Institutes of Health, Bethesda, MD, USA). Mitochondrial fragmentation vs connectivity was determined by plotting length × width of several thousand mitochondria from 12 randomly selected fields for each 10 cells were counted. At least 120 cells per group were counted[29].

Echocardiography

A transthoracic echocardiography was carried out on conscious, gently restrained mice using a Vevo 3100 system (VisualSonics, Ontario, Canada). Male mice were anesthetized with 1.5–3% isoflurane in 100% oxygen at different time points post-MI. The left ventricle (LV) was assessed using the

Fig. 5 | Overexpression of *Klf7* aggravates cardiomyocyte mitochondrial dynamics imbalance and insufficient ATP supply under hypoxic condition. **a**–**c** Oxygen consumption rate, ATP production, and maximal respiration rate of HL-1 cells under 1 mM H_2O_2 treatment ($n = 5$). **d** NMCMs were stained with MitoTracker Red (red)/DAPI (blue). Representative images highlight mitochondrial fission/fusion dynamics. Scale bar, 10 μm. **e**, **f** Quantitative analysis was performed to determine the percentage of cells with altered mitochondrial aspect ratios and fragmented mitochondria ($n = 12$). **g** HL-1 cells were transfected with lentivirus overexpressing *Klf7* or its negative control. Apoptosis was determined by the TUNEL assay. DAPI indicates the nucleus. Scale bar, 50 μm. Quantitative analysis was conducted to determine the percentage of apoptotic cells, based on 12 randomly selected fields from 4 independent experiments. **h** Cell apoptosis evaluated by the Annexin V-FITC/PI staining of cardiomyocytes with lentiviral overexpression of *Klf7* exposed to hypoxic conditions for 12 h ($n = 5$). The x-axis labeled Comp-FITC-A indicates Annexin V, while the y-axis labeled Comp-PE-A indicates PI. In all panels, data are depicted as the mean ± SEM. $^{*}P < 0.05$, $^{***}P < 0.001$, $^{****}P < 0.0001$, statistical significance was determined using unpaired, two-sided t-test.

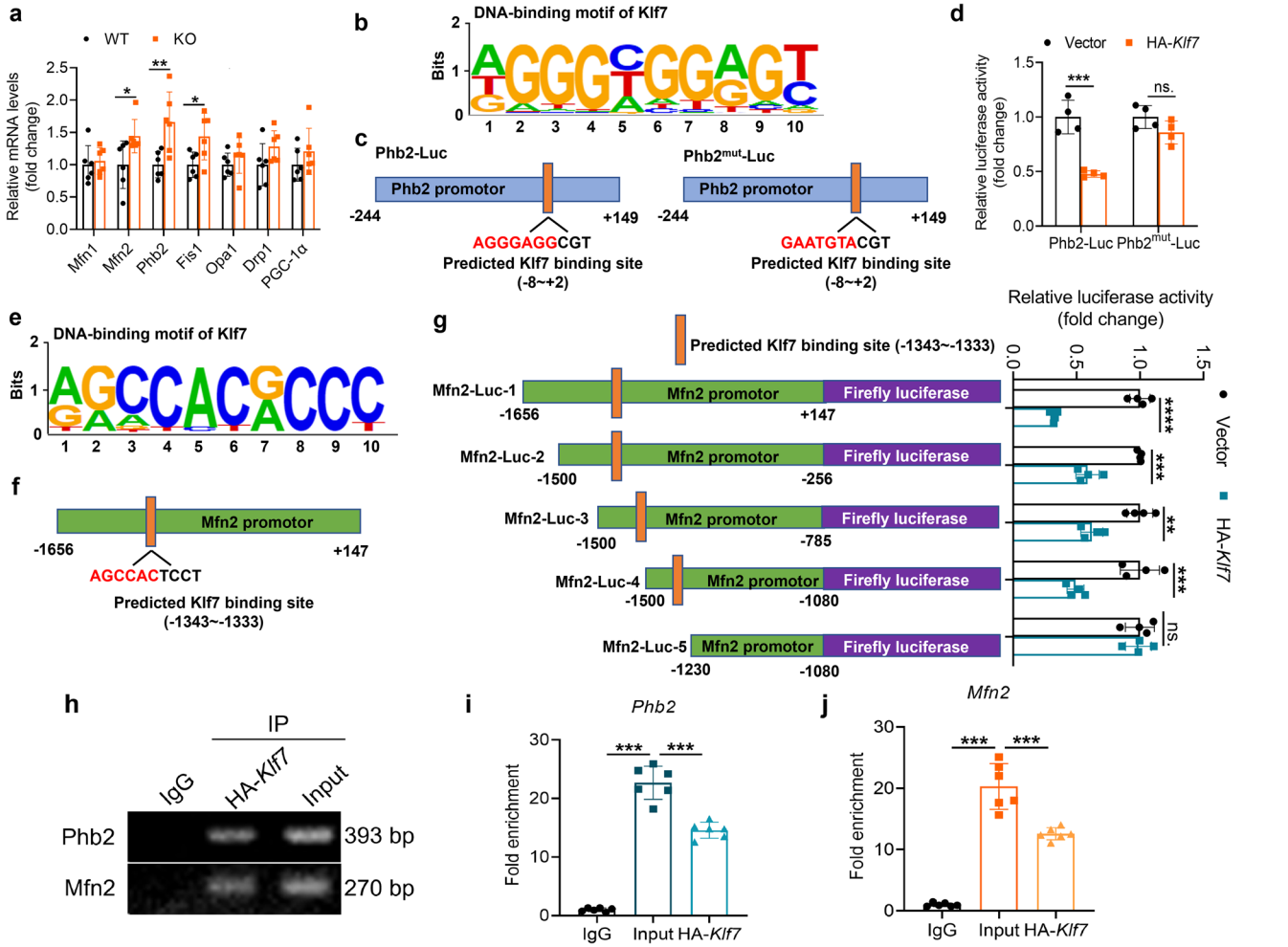

Fig. 6 | *Mfn2 and Phb2* function as direct targets of *Klf7* in cardiac mitochondrial dynamics. **a** Quantitative analysis of mRNA expression levels of genes involved in mitochondrial dynamics in the heart tissues of WT and *Klf7* KO mice ($n = 6$). **b**, **c** The *Klf7* DNA binding motif and mutation sequence diagram of the *Phb2* promoter predicted by ChIP-seq. **d** *Klf7* negatively regulates *Phb2* expression as quantified by luciferase reporter assay ($n = 4$). **e**, **f** The *Klf7* DNA binding motif and schematic diagram of the *Mfn2* promoter predicted by ChIP-seq. **g** The *Mfn2* promoter region (−1500–−1230) acts as a *Klf7*-targeting binding region. *Klf7* negatively regulates *Mfn2* expression as quantified by luciferase reporter assay ($n = 4$). **h**–**j** ChIP-PCR performed upon negative control lentivirus (lenti-NC) transfection or lentivirus-mediated HA-*Klf7* overexpression in HL-1 cells confirmed that *Klf7* binds the promotor regions of the *Mfn2* and *Phb2* genes ($n = 6$). In all panels, data are presented as mean ± SEM. $^{*}P < 0.05$, $^{**}P < 0.01$, $^{***}P < 0.001$, $^{****}P < 0.0001$, statistical significance was determined using unpaired, two-sided t-test.

parasternal long-axis view. The LV wall thickness, LV diameter, LV volume, ejection fraction, and fractional shortening were measured in M-mode at 1 kHz at the papillary muscle level.

Myocardial infarction surgery

Male mice (8–10 weeks old) of the respective genotypes with normal ejection fraction (EF) or fraction shortening (FS) were subjected to left anterior descending coronary artery ligation. Anesthesia of mice was achieved with 1.5–3% isoflurane in 100% oxygen. Then, the cheats of mice were opened to expose their hearts. The left descending coronary artery was ligated with a 7/0 nylon suture, 2 mm below the border between the left atrium and ventricle, to create the MI model. The mice in the sham-operated control group underwent the same experimental procedures as the MI group, but without undergoing ligation. At defined time points, mice were euthanized by CO_2 overdose at a flow rate of 10–30% of the cage volume per minute, and whole hearts or left ventricle infarct borders and remote areas were collected for histological, molecular, and biochemical analyses.

AAV9 infection

To achieve *Mfn2* and *Phb2* knockdown in the hearts of KO mice and WT littermates, AAV9 carrying shRNA to interfere with the *Mfn2* and *Phb2* genes was constructed and inserted into the GV683 vectors, and AAV9

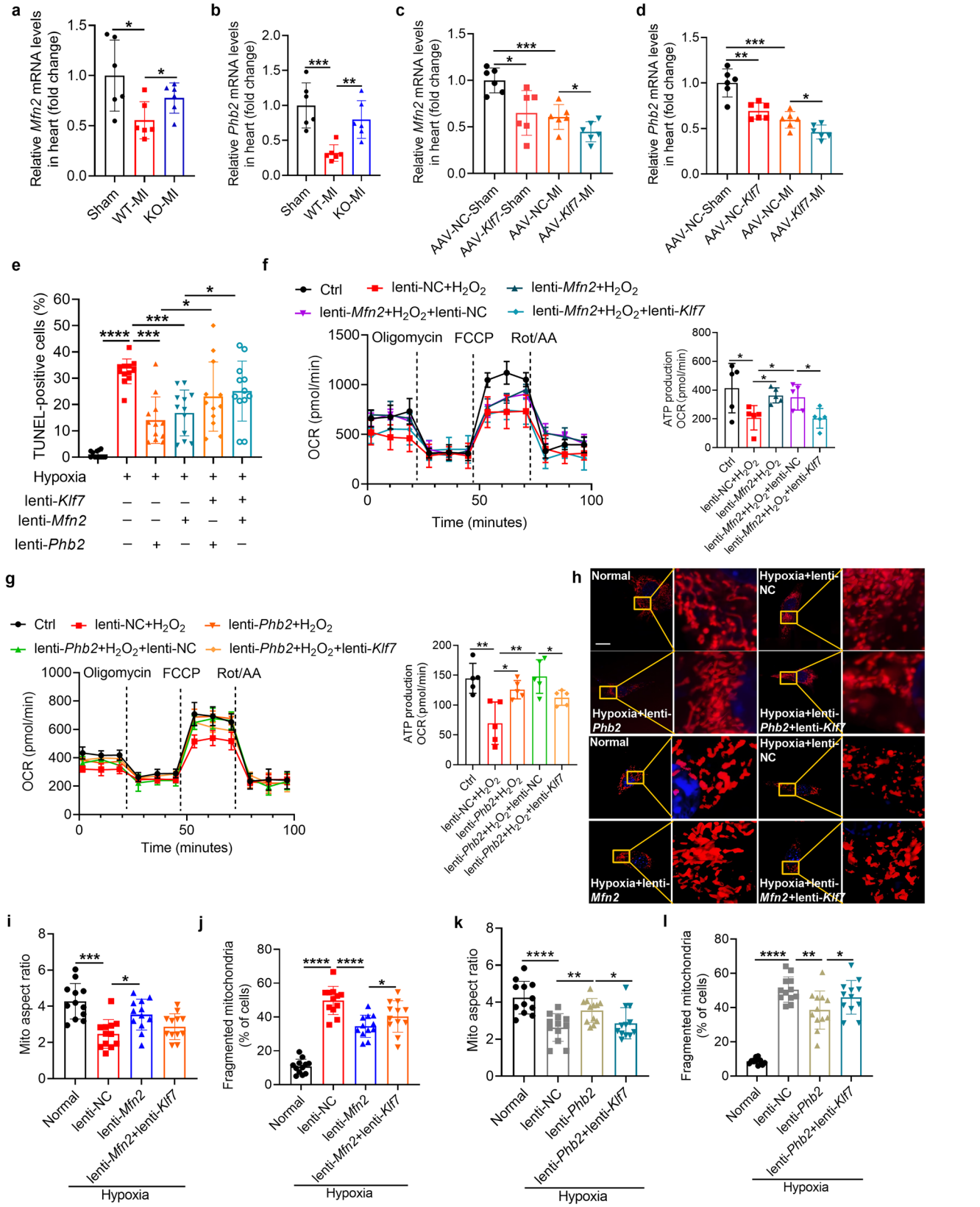

Fig. 7 | *Klf7* regulates mitochondrial fission and fusion by targeting *Mfn2 and Phb2*. **a**, **b** Cardiomyocyte expression levels of *Mfn2* and *Phb2* in WT or *Klf7* KO mice subjected to MI determined by qRT-PCR ($n = 6$). **c**, **d** Overexpression of *Klf7* aggravates the MI-induced decrease in *Mfn2* and *Phb2* expression as assessed by qRT-PCR ($n = 6$). **e** TUNEL staining of HL-1 cells and the percentage of TUNEL-positive HL-1 cells (green) were quantified, Scale bar, 50 μm (12 randomly selected fields from 4 independent experiments). **f**, **g** Oxygen consumption rate and ATP production determined by the Seahorse XF24 analyzer in HL-1 cells under normal and hypoxic conditions in the five groups ($n = 5$). **h**–**l** NMCM mitochondria were stained with MitoTracker Red (red) and mitochondrial morphology was quantified. Scale bar, 10 μm ($n = 12$). In all panels, data are depicted as the mean ± SEM. $^{*}P < 0.05$, $^{**}P < 0.01$, $^{***}P < 0.001$, $^{****}P < 0.0001$, statistical significance was determined using unpaired, two-sided t-test.

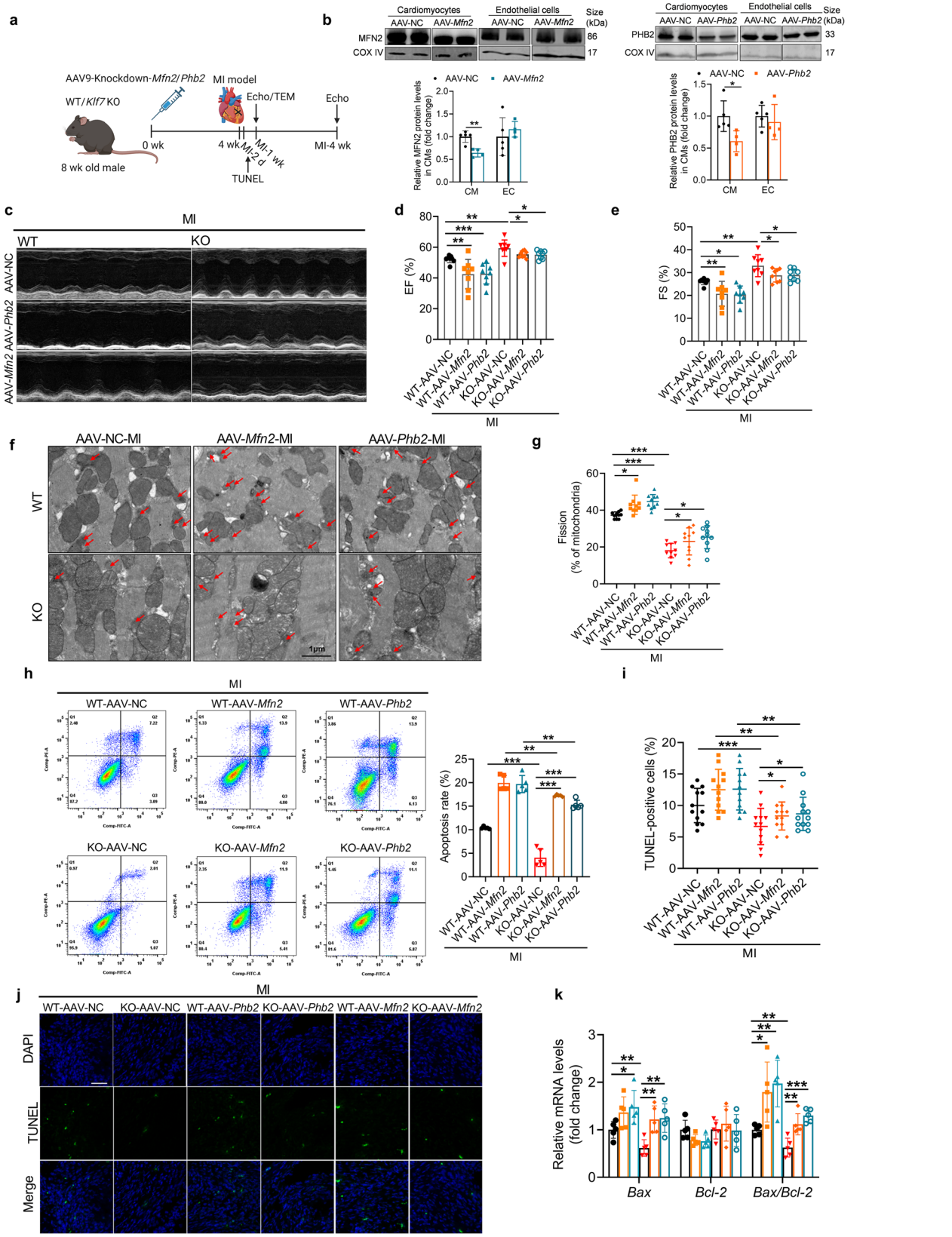

encoding GFP was used as a control. AAV9 particles were used to package the constructs and envelope plasmids in 293A cells. After 48 h of transfection, cell supernatants were collected and concentrated using ultracentrifugation (Optima L-100XP, Beckman Coulter, CA, USA) to obtain viral particles. The resulting stocks were resuspended in a serum-free culture medium and stored at −80 °C until needed. Two-month-old KO and WT mice were treated with AAV9 3E + 11 particles per mice via tail vein injection. AAV9 was purchased from GeneChem (Shanghai, China) (AAV9.sh*Phb2*, catalog no. GIDV0331036; AAV9.sh*Mfn2*, catalog no. GIDV0331895).

Fig. 8 | Cardiomyocyte-specific knockdown of *Mfn2* or *Phb2* aggravates *Klf7* KO mice cardiac function and mitochondria injury after myocardial infarction. **a** Schematic diagram of the strategy for the echocardiography (Echo) and mitochondrial dynamics analysis. 8-week-old male WT and *Klf7* KO mice were randomly grouped and then subjected to tail vein injection of AAV9-*Mfn2*/*Phb2* virus to induce *Mfn2*/*Phb2* knockdown. **b** Infection efficiency upon mouse tail-vein injection of AAV9 for Mfn2 and Phb2 expression in heart cardiomyocytes (CMs) and endothelial cells (ECs) (AAV-NC, $n = 5$; AAV-*Mfn2*/*Phb2*, $n = 4$). **c** An illustration of the ventricle's long-axis image, with the traced area displaying the heart's wall movement, and the measurement of EF (**d**), FS (**e**) in *Klf7* KO mice 1 week post-MI ($n = 8$). **f**, **g** TEM was performed to detect the ultrastructure of cardiomyocytes in heart tissues from mice treated with AAV-*Mfn2*/*Phb2* or AAV-NC in WT or *Klf7* KO mice after MI surgery. Red arrows indicate fragmented mitochondria. Scale bar, 1 μm ($n = 5$). **h** Cell apoptosis of cardiomyocytes in the border zone was determined by flow cytometry ($n = 5$). The x-axis labeled Comp-FITC-A indicates Annexin V, while the y-axis labeled Comp-PE-A indicates PI. **i**, **j** Apoptosis of cardiomyocytes in the border zone was determined by TUNEL staining. Scale bar, 100 μm ($n = 4$ mice/group, 3 sections/mouse). **k** The mRNA expression of apoptosis-relevant genes in *Klf7* KO mice after MI ($n = 5$). In all panels, data are depicted as the mean ± SEM. $^{*}P < 0.05$, $^{**}P < 0.01$, $^{***}P < 0.001$, statistical significance was determined using unpaired, two-sided t-test.

Neonatal mice cardiomyocytes isolation and lentivirus infection

Neonatal mice that were born 1–3 d prior were euthanized using CO_2 overdose at a flow rate of 10–30% of the cage volume per minute. Primary NMCMs were isolated and cultured in DMEM containing 10% fetal bovine serum (FBS, 04-001-1ACS, Biological Industries, Kibbutz Beit Haemek, Israel) and penicillin-streptomycin (Solarbio, Beijing, China). To perform lentivirus-mediated gene knockdown and overexpression, cells were incubated for 48 h infection with lentivirus. NMCMs were subsequently analyzed for infection efficiency by measuring the fluorescence of GFP. The shRNA plasmid was constructed by Genechem (Shanghai, China) (sh-*Klf7*; catalog no. GIEE0269089; sh-*Phb2*, catalog no. GIEE0331037).

Cell culture

A human ventricular cardiomyocyte-derived cell line, designated AC16, a mouse atrial cardiomyocyte-derived cell line, designated HL-1, and a human embryonic kidney cell 293 cell line, designated HEK293T were used for in vitro experiments. AC16 cells were maintained in DMEM:F12 (#SH30023.01; HyClone, Logan, UT, USA) supplemented with 10% FBS, 1% penicillin-streptomycin, and 1% fungizone (#C0222; Beyotime, Shanghai, China), HL-1 and HEK293T cells were maintained DMEM with 10% FBS and penicillin-streptomycin, and grown at 37 °C in a humid atmosphere of 5% CO_2 + 95% air until they had reached 70–80% confluence.

Whole-cell lysates from mouse left ventricles and NMCMs were prepared in radioimmunoprecipitation assay (RIPA) buffer (89901, Thermo Fisher Scientific) containing protease and phosphatase inhibitors (11836170001, Roche, Basel, Switzerland). Samples containing equal amounts of protein (10–20 μg) were separated on a 12% SDS-PAGE gel (Thermo Fisher Scientific), and transferred to a nitrocellulose membrane (Sigma-Aldrich, Waltham, MA, USA). Proteins were detected using primary antibodies against the following targets diluted 1,000-fold: Mfn2 (A12771; ABclonal, Wuhan, China), Phb2 (12295-1-AP; Proteintech, Wuhan, China), COX IV (AF5468, Affinity Biosciences, Cincinnati, OH, USA), KLF7 (H00008609-M01; Abnova, Taiwan, China), α-tubulin (AC007; ABclonal), and GAPDH (10R-G109a; Fitzgerald Industries, Acton, MA, USA). After washing, membranes were incubated with secondary antibodies (AS014/AS003, ABclonal), after which specific protein bands were detected and quantified using an Odyssey scanner (version 3, LI-COR Biosciences, Lincoln, NE, USA). The intensity of the bands was quantified using ImageJ software.

Histology and immunohistochemistry

Histological and immunohistochemical (IHC) analyses were carried out on formaldehyde-fixed hearts that were processed for generating frozen sections as per the standard protocol. Briefly, hearts were fixed in 4% paraformaldehyde overnight at 4 °C and transferred to 1×PBS (Solarbio, Beijing, China), followed by optimal cutting temperature compound (OTC) embedding. Haematoxylin and eosin (H&E, Solarbio, Beijing, China) and Masson's trichrome staining (Solarbio, Beijing, China) was performed for morphological and fibrosis analyses. The fibrotic area fraction was obtained by using automated image analysis (Image-Pro Plus, Media Cybernetics, Rockville, MD, USA).

Luciferase and ChIP-PCR assay

Based on our previous ChIP-seq database on mouse overexpression of *Klf7*[24], we learned that *Klf7* can target the promoter binding sequence of *Mfn2* and *Phb2*, and then conducted luciferase assay and ChIP-PCR assay to verify this. The promotor regions of *Mfn2* and *Phb2* were cloned into the KpnI and HindIII restriction sites of a plasmid containing a luciferase reporter and the PGL4 basic vector. Luciferase activity was quantified in lysates of HEK293T cells transfected with PGL4-*Phb2* and PGL4-*Mfn2* containing fragments of *Mfn2* and *Phb2* promoters, and infected with overexpression *Klf7* for 48 h. Luciferase activity was measured using Dual-Luciferase Reporter Assay System (E1910; Promega, Madison, Wisconsin, USA) and was normalized to Renilla activity.

The quantitative analysis of the ChIP-PCR assays was carried out as previously described[24]. Briefly, HL-1 cells overexpressing HA-tagged *Klf7* were processed using the Zymo-Spin ChIP kit (D5210, Zymo Research, CA, USA) according to the manufacturer's instructions, enabling KLF7 to be immunoprecipitated with an HA-tag antibody. HA-tag acts as a tag-specific antibody to obtain the target protein-DNA complex. DNA was purified, and PCR amplification was performed using primers targeting the *Phb2* or *Mfn2* promoter regions. The resulting gel bands were then assessed. The primers for the sequences of luciferase and the ChIP-PCR assay were as follows: *Phb2*, forward 5′-GGGGTACCTTTAACAGTCTATGACGAGTACTTT-3′ and reverse 5′-CCGCTCGAGGAAGGTTGGGATGGAGGCAAGCTCA-3′; *Mfn2*, forward 5′-GGGGTACCAATCTCTAGTCAGTTTTC-CAAAGGG-3′ and reverse 5′-CCAAGCTTCAGTAAATGGTTAGAAA-CACTCCCT -3′.

RNA extraction and quantitative real-time PCR (qRT-PCR)

Total RNA was isolated from mouse hearts and NMCMs using TRIzol reagent (15596026; Invitrogen, Waltham, MA, USA) according to the manufacturer's protocol. cDNA was synthesized using the ReverTra Ace qPCR RT reagent kit (FSQ-301; TOYOBO, Osaka, Japan) according to the manufacturer's instructions, and gene expression was analyzed by qPCR using the SYBR Green Master Mix (50837000; Roche) on a ViiA 7 real-time PCR system (ABI, Carlsbad, CA, USA) according to the manufacturer's instructions. Primer sequences used for each reaction are listed in Supplementary Table 1.

Mitochondrial DNA content

The Genomic DNA Isolation Kit (ab65358, Abcam, Cambridge, UK) was used to extract the mice heart tissue genomic DNAs according to the manufacturer's instructions. Routine PCR reactions were performed with SYBR Green Master Mix (50837000; Roche) on a real-time PCR system (ABI) to detect relative amount of mitochondrial DNA. Primer sequences used for the reaction was as follows: forward 5′-TCGCCTACTCCT-CAGTTAGC-3′ and reverse 5′- TCCGTTCGTAGTTGGAGTTTG -3′.

Measurement of infarct size

Heart tissue was first divided into five biventricular sections of equal thickness and then taken and stored at −80 °C for 1 h. Five sections were cut from the apex of the largest lumen of the heart, placed in 1.5% triphenyltetrazolium chloride (TTC, Sigma-Aldrich, Waltham, MA, USA), dissolved in saline, and stored at 37 °C in the dark for 30 min. The white regions

represented infarcted tissue and were quantified under a digital camera with ImageJ software. The myocardial infarct size was measured as the percentage of the infarct area with respect to the total ventricular area.

TUNEL assay

Cardiomyocyte apoptosis were assessed in vivo and in vitro using an in situ apoptosis detection kit (Roche) by the indirect terminal deoxynulceotidyl transferase nick-end-labeling (TUNEL) method, according to the manufacturer's instructions. Nuclei were stained with DAPI (Solarbio, Beijing, China). Immunofluorescence was analyzed using a fluorescence microscope (LSM880, Carl Zeiss). The number of TUNEL-positive cardiomyocytes (HL-1) was counted in 12 randomly selected fields, each group consisted of 4 mice or 4 cardiomyocyte parallel samples. The percentage of apoptotic cells was determined by the ratio of apoptotic cells to total cells.

Flow cytometry

Cardiomyocyte apoptosis was performed using a FITC Annexin V Apoptosis Detection Kit I (BD Pharmingen, San Jose, CA, USA) according to the manufacturer's protocol. Cells were collected and washed twice with cold PBS. The cells were then re-suspended in 1× Binding Buffer at a concentration of 1 ×10E6 cells/ml., after which 5 μL Annexin V and 5 μL propidium iodide (PI) were mixed evenly, and the mixture was incubated in the dark for 15 min. The cells were then assessed by flow cytometry. The apoptosis rate (%) was calculated as [Annexin V (+) PI (−) cells + Annexin V (+) PI (+) cells]/total number of cells ×100.

Electron microscopy

Heart sample preparations and electron microscopy were performed as described before[60]. In brief, hearts excised from mice were fixed in 2.5% glutaraldehyde (Sigma-Aldrich, Waltham, MA, USA) and 0.1 M sodium cacodylate (Sigma-Aldrich, Waltham, MA, USA) buffer at 4 °C overnight followed by obtaining a 2 mm transverse slice, 3 mm from the apex, from each heart. Ultrathin sections were examined with a JEM-1230 transmission electron microscope (TEM) (JEOL, Tokyo, Japan). The TEM allowed mitochondria to be observed at ×6000 magnification. The size of individual mitochondrion was measured by using Image-Pro Plus software (Midia Cybernetics, Rockville, MD, USA). Approximately 800–1000 mitochondria were measured to determine the percentages of mitochondria with various sizes. In MI-treated heart tissues, mitochondria disintegrated into numerous small round fragments of varying size and the number of small mitochondria was increasing. Thus, we categorized mitochondria smaller than 0.6 μm^2 as having undergone fission. Data represent mean ± standard error of the mean (SEM). of at least six independent experiments.

Isolation of mitochondria from heart tissue

Mitochondria were isolated from mouse heart tissue using the Mitochondria Isolation Kit for Tissue (Abcam; ab110168) according to the manufacturer's instructions. Briefly, mice were euthanized, the heart tissue was immediately washed in ice-cold PBS buffer, and cut into small pieces using scissors. The sample tissue was washed twice with wash buffer, minced with 1 ml Dounce homogenizer, and then each tube was filled with isolation buffer. The homogenate was centrifuged at 1000 × *g* for 10 min at 4 °C. The supernatant was transferred into a centrifugation tube and centrifuged at 12,000 × *g* for 15 min at 4 °C, and the pellet was resuspended in 500 μL of isolation buffer supplemented with 5 μL protease inhibitor cocktail (Solarbio). The crude mitochondrial fraction pellet was utilized to quantify mitochondrial protein.

Isolation of mitochondria from cardiomyocytes

Mitochondria were isolated from cardiomyocytes using the Cell Mitochondria Isolation Kit (C3601, Beyotime) according to the manufacturer's instructions. Cardiomyocytes were digested and collected by 0.25% pancreatic enzyme (Solarbio, Beijing, China). A small number of cells were counted, and 1.0–2.5 mL of mitochondria isolation reagent was added to 2–5E7 cardiomyocytes and placed on ice for 15 min. Then the cells were transferred to a glass homogenizer and homogenized using about 10–30 strokes. The cell homogenates were centrifuged at 600 × *g* for 10 min at 4 °C. The supernatant was transferred to another centrifugation tube and centrifuged at 11,000 × *g* and 4 °C for 10 min. The supernatant was carefully removed. The precipitate is the isolated cardiomyocyte mitochondrial fraction.

Measurement of cardiac mitochondria oxygen consumption rate

The oxygen consumption rate (OCR) of mouse heart tissue and cardiomyocyte (HL-1) mitochondria were detected with a Seahorse XF24 Analyzer (Agilent Technologies, Santa Clara, CA, USA). The Agilent Mito Stress Test Kit was used to determine the OCR. On the day prior experimentation, the sensor cartridge was hydrated in a 37 °C non-CO_2 incubator and cardiomyocytes were seeded at the desired final concentration (5 μg/50 μL). The cell culture microplate was centrifuged at 2000 × *g* for 20 min at 4 °C. After centrifugation, 150 μL of mitochondrial assay buffer (MAS) containing pyruvate/malate was added to each well and incubated for 10 min in a non-CO_2 incubator. Fresh aliquots were used to prepare the working solutions. Working drug (oligomycin, carbonyl cyanide 4-(trifluoromethoxy) phenylhydrazone (FCCP), and antimycin/rotenone (Rot/A)) solutions were prepared in the required quantities every day in pH-adjusted MAS containing pyruvate and malate. Following microplate insertion, the XF24 protocol consisted of baseline and stepwise injection measurements (3 min for mix, 2 min for incubation, and 3 min for measurement for a total of three cycles).

Statistics and reproducibility

All data are presented as mean ± SEM. GraphPad Prism software (version 8.0) (GraphPad Software, Boston, MA, USA) was used for the statistical analysis. All experiments were performed with at least four biological replicates. The exact number of biological replicates (number of mice, samples, or cell culture dishes) is indicated in the figure legends. A two-tailed independent sample t-test was used to compare the differences in mean values between the two groups. A result was considered statistically significant if the $P < 0.05$.

Reporting summary

Further information on research design is available in the Nature Portfolio Reporting Summary linked to this article.

Data availability

The source data behind the graphs are available in zenodo (https://doi.org/10.5281/zenodo.15227857). The newly generated plasmid deposit in the Addgene database (AAV-*Mfn2*: 238882, AAV-*Phb2*: 238883, Lenti-*Phb2*: 238886, Lenti-*Mfn2*: 238887, *Phb2*-luc: 238888, *Phb2*-mut-Luc: 238898, *Mfn2*-luc-1: 238889, *Mfn2*-luc-2: 238890, *Mfn2*-luc-3: 238891, *Mfn2*-luc-4: 238892, *Mfn2*-luc-5: 238893, sh-*Klf7*: 238895, AAV-*Klf7*: 238896, Lenti-*Klf7*: 238897). Other data are available from the corresponding author on reasonable request.

Received: 23 July 2024; Accepted: 28 April 2025;
Published online: 09 May 2025

References

1. Reed, G. W., Rossi, J. E. & Cannon, C. P. Acute myocardial infarction. *Lancet* **389**, 197–210 (2017).
2. Quiles, J. & Gustafsson, A. The role of mitochondrial fission in cardiovascular health and disease. *Nat. Rev. Cardiol.* **19**, 723–736 (2022).
3. Wai, T. et al. Imbalanced OPA1 processing and mitochondrial fragmentation cause heart failure in mice. *Science* **350**, 0116 (2015).
4. Bonora, M. et al. Targeting mitochondria for cardiovascular disorders: therapeutic potential and obstacles. *Nat. Rev. Cardiol.* **16**, 33–55 (2018).

5. Chaanine, A. H. et al. Mitochondrial Morphology, Dynamics, and Function in Human Pressure Overload or Ischemic Heart Disease With Preserved or Reduced Ejection Fraction. *Circ. Heart Fail.* **12**, 005131 (2019).
6. Ahuja, P. et al. Divergent Mitochondrial Biogenesis Responses in Human Cardiomyopathy. *Circulation* **127**, 1957–1967 (2013).
7. Ong, S. B. et al. Inhibiting Mitochondrial Fission Protects the Heart Against Ischemia/Reperfusion Injury. *Circulation* **121**, 2012–2022 (2010).
8. Giampaolo, M. et al. Comprehensive Analysis of Mitochondrial Dynamics Alterations in Heart. *Int. J. Mol. Sci.* **24**, 1–25 (2023).
9. Rehman, J. Empowering self-renewal and differentiation: the role of mitochondria in stem cells. *J. Mol. Med.* **88**, 981–986 (2010).
10. Atsuko, K. et al. Mitochondrial Fusion Directs Cardiomyocyte Differentiation via Calcineurin and Notch Signaling. *Science* **342**, 6159 (2013).
11. Chen, Y., Liu, Y. & Dorn, G. W. Mitochondrial Fusion is Essential for Organelle Function and Cardiac Homeostasis. *Circ. Res.* **109**, 1327–1331 (2011).
12. Mishra, P. & Chan, D. C. Mitochondrial dynamics and inheritance during cell division, development and disease. *Nat. Rev. Mol. Cell Biol.* **15**, 634–646 (2014).
13. Wong, W. Breaking mitochondria and hearts. *Science* **362**, 778–790 (2018).
14. Wang, J. X. et al. miR-499 regulates mitochondrial dynamics by targeting calcineurin and dynamin-related protein-1. *Nat. Med.* **17**, 71–78 (2010).
15. Ong, S. B. et al. Targeting Mitochondrial Fission Using Mdivi-1 in A Clinically Relevant Large Animal Model of Acute Myocardial Infarction: A Pilot Study. *Int. J. Mol. Sci.* **20**, 3972 (2019).
16. Disatnik, M. H. et al. Acute Inhibition of Excessive Mitochondrial Fission After Myocardial Infarction Prevents Long-term Cardiac Dysfunction. *J. Am. Heart Assoc.* **2**, 000461 (2013).
17. Zhou, H., RolRen, J., Toan, S. & Mui, D. Role of mitochondrial quality surveillance in myocardial infarction: From bench to bedside. *Ageing Res. Rev.* **66**, 101250 (2021).
18. Michael, C. et al. Physiologic Mitochondrial Fragmentation Is a Normal Cardiac Adaptation to IncreasedEnergy Demand. *Circ. Res.* **122**, 282–295 (2017).
19. Piamsiri, C. et al. Chronic mitochondrial fusion promotor as a novel pharmacological intervention to alleviate left ventricular dysfunction in rats with chronic myocardial infarction. *Eur. Heart J.* **43**, ehac544.960 (2022).
20. Cooper, H. A. & Eguchi, S. Inhibition of mitochondrial fission as a noveltherapeutic strategy to reduce mortality uponmyocardial infarction. *Clin. Sci.* **132**, 2163–2167 (2018).
21. Ikeda, Y. et al. Endogenous Drp1 Mediates Mitochondrial Autophagy and Protects the Heart Against Energy Stress. *Circ. Res.* **116**, 264–278 (2015).
22. Song, M., Franco, A., Fleischer, J. A., Zhang, L. & Dorn, G. W. Abrogating Mitochondrial Dynamics in Mouse Hearts Accelerates Mitochondrial Senescence. *Cell Metab.* **26**, 872–883 (2017).
23. Ong, S. B., Kalkhoran, S. B., Cabrera-Fuentes, H. A. & Hausenloy Derek, J. Mitochondrial fusion and fission proteins as novel therapeutic targets for treating cardiovascular disease. *Eur. J. Pharmacol.* **763**, 104–114 (2015).
24. Wang, C. et al. The KLF7/PFKL/ACADL axis modulates cardiac metabolic remodelling during cardiac hypertrophy in male mice. *Nat. Commun.* **14**, 959 (2023).
25. Cheng, W. C. et al. Expression data from aortic wall between myocardial infarction (MI) and non-MI group [Data set]. Gene Expression Omnibus, https://www.ncbi.nlm.nih.gov/geo/query/acc.cgi?acc=GSE83500 (2017).
26. Papanicolaou, K. N. et al. Mitofusin-2 Maintains Mitochondrial Structure and Contributes to Stress-Induced Permeability Transition in Cardiac Myocytes. *Mol. Cell. Biol.* **31**, 1309–1328 (2023).
27. Chen, L., Gong, Q., Stice, J. P. & Knowlton, A. A. Mitochondrial OPA1, apoptosis, and heart failure. *Cardiovasc. Res.* **84**, 91–99 (2009).
28. Hui, T. ChIP-seq of HA-tagged klf7 in N2A cells (klf7-rep2) [Data set]. *Zenodo*, https://zenodo.org/records/5243430 (2021).
29. Wang, J. et al. Bax inhibitor 1 preserves mitochondrial homeostasis in acute kidney injury through promoting mitochondrial retention of PHB2. *Theranostics* **10**, 384–397 (2020).
30. Merkwirth, C. et al. Prohibitins control cell proliferation and apoptosis by regulating OPA1-dependent cristae morphogenesis in mitochondria. *Genes Dev.* **22**, 476–488 (2008).
31. Wei, Y., Chiang, W. C., Sumpter, R. Jr., Mishra, P. & Levine, B. Prohibitin 2 Is an Inner Mitochondrial Membrane Mitophagy Receptor. *Cell* **168**, 224–238 (2017).
32. Lahiri, V. & Klionsky, D. J. PHB2/prohibitin 2: An inner membrane mitophagy receptor. *Cell Res.* **27**, 311–312 (2017).
33. Wang, K. et al. CARL lncRNA inhibits anoxia-induced mitochondrial fission and apoptosis in cardiomyocytes by impairing miR-539-dependent PHB2 downregulation. *Nat. Commun.* **5**, 3596 (2014).
34. Chen, Y. & Dorn, G. W. PINK1-Phosphorylated Mitofusin 2 Is a Parkin Receptor for Culling Damaged Mitochondria. *Science* **340**, 471–475 (2013).
35. Liu, X., Guo, C. & Zhang, Q. Novel insights into the involvement of mitochondrial fission/fusion in heart failure: From molecular mechanisms to targeted therapies. *Cell Stress Chaperones.* **28**, 133–144 (2023).
36. Brown, D. A. et al. Mitochondrial function as a therapeutic target in heart failure. *Nat. Rev. Cardiol.* **14**, 238–250 (2016).
37. Vásquez-Trincado, C. et al. Mitochondrial dynamics, mitophagy and cardiovascular disease. *J. Physiol.* **594**, 509–525 (2016).
38. Ding, M. et al. Mfn2-mediated mitochondrial fusion alleviates doxorubicin-induced cardiotoxicity with enhancing its anticancer activity through metabolic switch. *Redox Biol.* **52**, 102311 (2022).
39. Palee, S., Higgins L., Leech T., Chattipakorn, S. C. & Chattipakorn, N. Metformin exerts cardioprotection via attenuating mitochondrial fission in cardiac. *Eur. Heart J.* **41**, 110604 (2020).
40. Aishwarya, R. et al. Pleiotropic effects of mdivi-1 in altering mitochondrial dynamics, respiration, and autophagy in cardiomyocytes. *Redox Biol.* **36**, 101660 (2020).
41. Maneechote, C. et al. Balancing mitochondrial dynamics via increasing mitochondrial fusion attenuates infarct size and left ventricular dysfunction in rats with cardiac ischemia/reperfusion injury. *Clin. Sci.* **133**, CS20190014–CS20190513 (2019).
42. Crunkhorn, S. Targeting transcription factors. *Nat. Rev. Drug Discov.* **18**, 18–25 (2018).
43. Alexanian, M. et al. A transcriptional switch governs fibroblast activation in heart disease. *Nature* **595**, 1–6 (2021).
44. Sano, M. et al. Activation and function of cyclin T-Cdk9 (positive transcription elongation factor-b) in cardiac muscle-cell hypertrophy. *Nat. Med.* **8**, 1310–1317 (2002).
45. Lee, T. M., Lin, M. S. & Chang, N.-C. Inhibition of histone deacetylase on ventricular remodeling in infarcted rats. *Am. J. Physiol. Heart Circ. Physiol.* **293**, 68–77 (2007).
46. Zhang, Q. et al. Signaling pathways and targeted therapy for myocardial infarction. *Sig. Transduct. Target. Ther.* **7**, 78 (2022).
47. Hu, H. et al. AnimalTFDB 3.0: a comprehensive resource for annotation and prediction of animal transcription factors [Data set]. Human Transcription Factor Database http://bioinfo.life.hust.edu.cn/HumanTFDB/#! (2019).
48. Lee, K. C. Y. et al. PKM2 regulates metabolic flux and oxidative stress in the murine heart [Data set]. Gene Expression Omnibus https://www.ncbi.nlm.nih.gov/geo/query/acc.cgi?acc=GSE243668 (2024).

49. Lee, K. C. Y. et al. Loss of PKM2 dysregulates inflammatory signaling in the infarcted murine heart [Data set]. Gene Expression Omnibus https://www.ncbi.nlm.nih.gov/geo/query/acc.cgi?acc=GSE243668 (2025).
50. Li, S. et al. A Humanized Monoclonal Antibody Targeting an Ectonucleotidase Rescues Heart Function after Myocardial Infarction [Data set]. Gene Expression Omnibus https://www.ncbi.nlm.nih.gov/geo/query/acc.cgi?acc=GSE255826 (2024).
51. Nikolaou, P. E. et al. Empagliflozin in Acute Myocardial Infarction Reduces No-Reflow and Preserves Cardiac Function by Preventing Endothelial Damage [Data set]. Gene Expression Omnibus https://www.ncbi.nlm.nih.gov/geo/query/acc.cgi?acc=GSE255933 (2024).
52. Hoffman, M. et al. Cardiomyocyte Krüppel-Like Factor 5 Promotes De Novo Ceramide Biosynthesis and Contributes to Eccentric Remodeling in Ischemic Cardiomyopathy. *Circulation* **143**, 1139–1156 (2021).

Acknowledgements

This work was supported by the National Natural Science Foundation of China (82400320), the Postdoctoral Fellowship Program of CPSF (GZC20242212), China Postdoctoral Science Foundation (2024M764164), Postdoctoral Fellowship of Heilongjiang Province (LBH-Z24017) and the Fundamental Research Funds for the Central Universities (HIT.DZJJ.2023129). We would like to express their gratitude to EditSprings (https://www.editsprings.cn) for the expert linguistic services provided.

Author contributions

T.W.M. L.J., and W.C. designed the experiments and supervised the study. W.C., Z.F.X., Z.L., Z.S.T., T.H., and W.J.H., performed the majority of the biochemical experiments. W.C., Z.B.S., X.X., J.R.X., H.X.L., and W.R.Q. performed animal experiments. W.C., L. J., and T.W.M. wrote and edited the manuscript.

Competing interests

The authors declare no competing interests.

Additional information

Supplementary information The online version contains supplementary material available at https://doi.org/10.1038/s42003-025-08139-z.

Correspondence and requests for materials should be addressed to Weiming Tian.

Peer review information *Communications Biology* thanks Santosh Karnewar, Mirko Völkers, Chad Grueter and the other, anonymous, reviewer(s) for their contribution to the peer review of this work. Primary Handling Editor: Christina Karlsson Rosenthal. A peer review file is available.